

Heavy neutral leptons from kaons in effective field theory

Rebeca Beltrán,^a Julian Günther,^b Martin Hirsch,^a Arsenii Titov,^c
Zeren Simon Wang^{d,e}

^a*AHEP Group, Instituto de Física Corpuscular – CSIC/Universitat de València, Apartado 22085, E-46071 València, Spain*

^b*Bethe Center for Theoretical Physics & Physikalisches Institut der Universität Bonn, Nußallee 12, 53115 Bonn, Germany*

^c*Dipartimento di Fisica “Enrico Fermi”, Università di Pisa and INFN, Sezione di Pisa, Largo Bruno Pontecorvo 3, I-56127 Pisa, Italy*

^d*Department of Physics, National Tsing Hua University, Hsinchu 300, Taiwan*

^e*Center for Theory and Computation, National Tsing Hua University, Hsinchu 300, Taiwan*

*E-mail: rebeca.beltran@ific.uv.es, guenther@physik.uni-bonn.de,
mahirsch@ific.uv.es, arsenii.titov@df.unipi.it, wzs@mx.nthu.edu.tw*

ABSTRACT: In the framework of the low-energy effective theory containing in addition to the Standard Model fields heavy neutral leptons (HNLs), we compute the decay rates of neutral and charged kaons into HNLs. We consider both lepton-number-conserving and lepton-number-violating four-fermion operators, taking into account also the contribution of active-heavy neutrino mixing. Assuming that the produced HNLs are long-lived, we perform simulations and calculate the sensitivities of future long-lived-particle (LLP) detectors at the high-luminosity LHC to the considered scenario. When applicable, we also recast the existing bounds on the minimal mixing case obtained by NA62, T2K, and PS191. Our findings show that for some of the effective operators considered the future LLP detectors, in particular, MATHUSLA and ANUBIS, will probe (i) new parts of the parameter space spanned by HNL mass and active-heavy neutrino mixing, and (ii) new-physics scales in excess of 2000 TeV.

Contents

1	Introduction	1
2	HNLs from kaons in effective field theory	3
2.1	The neutral kaon system	3
2.2	Effective field theory with right-handed neutrinos	4
2.3	HNL production in kaon decays	5
3	Experiments and simulation	6
4	Results	11
5	Summary	16
A	Kaon decays into HNLs	18
A.1	Form factors	19
A.2	Two-body decays	19
A.3	Three-body decays	20
B	HNL decays	22

1 Introduction

A rich program of searches for long-lived particles (LLPs) is planned at the LHC in the next decades [1–3]. It envisions the construction of several dedicated experiments sensitive to decay lengths of $\mathcal{O}(1 - 100)$ m. Some LLP detectors, namely, FASER [4, 5] and MoEDAL-MAPP1 [6, 7], are already operational, whereas several more experiments are planned for the high-luminosity (HL) phase of the LHC. These include ANUBIS [8], CODEX-b [9], FACET [10], FASER2 [3], MoEDAL-MAPP2 [6, 7], and MATHUSLA [1, 11, 12].

LLPs are present in many models that can account for unresolved problems in particle physics and cosmology, such as the mechanism of neutrino mass generation and the nature of dark matter. The main focus of phenomenological studies so far has been on various renormalizable models, including the Higgs portal, the neutrino portal, the dark photon portal, as well as on non-renormalizable models featuring long-lived axion-like particles (ALPs), see *e.g.* Refs. [3, 13] for reviews and references.

However, it is plausible that in addition to the renormalizable couplings, LLPs may interact with the Standard Model (SM) via effective, non-renormalizable interactions. In this case, the SM viewed as an effective field theory (EFT) has to be extended to include

LLPs and their effective interactions. One such example is the N_R SMEFT [14–17], which assumes the existence of heavy neutral leptons (HNLs), N , with masses below or around the electroweak scale, v . Recently, a dictionary of tree-level UV completions of the dimension-six and dimension-seven operators with N_R has been provided in Ref. [18].

There are two basic ways of HNL production at the LHC: (i) directly from partonic collisions, and (ii) for $m_N \leq$ (few) GeV, in decays of mesons, which in turn are copiously produced in pp collisions. The long-lived HNLs produced in the first way via the four-fermion operators with two quarks and either two or one N_R have been studied in Ref. [19] and Ref. [20], respectively. These two sets of effective operators lead to distinct phenomenology. The pair- N_R operators may enhance the production cross section while not contributing to the decay of the lightest HNL. This makes the far LLP detectors introduced above an ideal place to probe such effective interactions [19]. On the contrary, single- N_R operators, if large enough to enhance the HNL production, will also induce HNL decays. Still, displaced-vertex searches at the local LHC detectors (ATLAS and CMS) are very efficient to probe this set of effective operators [20]. The reach of the LLP detectors to the neutrino dipole operator involving an active neutrino and N_R has been recently estimated in Ref. [21]. Instead, Ref. [22] has revisited the LEP limits on the dimension-five sterile neutrino dipole operator (existing for at least two generations of HNLs, N_1 and N_2), taking into account active-heavy neutrino mixing.

Meson decays into long-lived HNLs triggered by non-renormalizable interactions have been considered in Refs. [23–26]. The EFT appropriate for the description of meson decays is N_R LEFT [27–30], the low-energy theory where the top quark, the Higgs boson and the heavy $SU(2)_L$ gauge bosons are not present as dynamical degrees of freedom. In Ref. [23], the authors have investigated the reach of the proposed LHC far detectors to HNLs produced in the decays of D - and B -mesons via single- N_R operators with a charged lepton, demonstrating that the new physics scale, Λ , as high as 100 TeV could be probed by these detectors. The same set of single- N_R operators, but with the τ lepton, would lead to HNL production in τ decays at Belle II [31] (see also Ref. [32]). Pair- N_R operators triggering D - and B -meson decays have been thoroughly examined in Ref. [24]. It has been shown that for certain operators Λ as large as 300 TeV and active-heavy neutrino mixing squared, $|U_{eN}|^2$, as small as 10^{-15} could be tested by MATHUSLA, with the reach of ANUBIS being only a factor of a few smaller. In Ref. [25], the sensitivities of FASER2, FACET, ANUBIS, CODEX-b, and MAPP, to the dimension-five sterile neutrino dipole operator have been estimated. This operator leads to two-body decays of vector mesons into N_1 and N_2 mediated by a photon, γ , and a subsequent decay of the heavier HNL $N_2 \rightarrow N_1\gamma$. Similarly, the sensitivity reach of FASER2 and FACET to the dipole operator coupling an HNL to the photon has recently been investigated in Ref. [26] for the HNLs produced from meson decays.

In the present work, we perform state-of-the-art numerical simulations and derive the sensitivities of the future LLP detectors at the LHC to HNLs produced from neutral

and charged kaon decays in the N_R LEFT.¹ First, we study the scenario in which the HNL production is induced by pair- N_R operators, while the HNL decay proceeds via active-heavy neutrino mixing U_{eN} . Second, we investigate the case in which both HNL production and decay are induced by the same single- N_R operator structure, but with different quark flavor indices. Finally, we consider the situation where the production proceeds via a single- N_R operator as well as via U_{eN} , while the N decays via mixing only. We consider both lepton-number-conserving (LNC) and lepton-number-violating (LNV) operators and discuss the differences.

HNLs can also mediate meson decays. In particular, LNV decays $K^\mp \rightarrow \pi^\pm \ell^\mp \ell^\mp$ mediated by light sterile neutrinos have been studied in Ref. [35] adopting the EFT approach. We also mention Ref. [36]. Here, the authors have derived limits on EFT operators from HNL searches in kaon decays (among others).

The remainder of the paper is organized as follows. In Sec. 2, we briefly recap neutral kaon mixing, summarize the N_R LEFT operators of interest, and then discuss the HNL production from kaon decays. In Sec. 3, we describe various experiments we consider and provide the details of numerical simulations. Sec. 4 contains the derived sensitivities and the relevant discussion. Finally, we provide summary and conclusions of our work in Sec. 5. Additionally, we add two appendices at the end of the paper which explain in detail the computation of the decay widths of the kaons into the HNLs and those of the HNLs into a charged lepton and a pion, in the EFT framework.

2 HNLs from kaons in effective field theory

2.1 The neutral kaon system

The neutral kaons K^0 ($d\bar{s}$) and \bar{K}^0 ($s\bar{d}$) are flavor eigenstates that can be produced in strong interactions. Weak interactions cause the mixing between these two neutral states. If CP were a symmetry of the total hamiltonian \mathcal{H} (including strong, electromagnetic, and weak interactions), CP eigenstates would also be eigenstates of \mathcal{H} . With the convention (see *e.g.* Ref. [37])

$$\widehat{CP}|K^0\rangle = -|\bar{K}^0\rangle, \quad \widehat{CP}|\bar{K}^0\rangle = -|K^0\rangle, \quad (2.1)$$

we can define the CP eigenstates as:

$$|K_1\rangle = \frac{1}{\sqrt{2}} \left(|K^0\rangle - |\bar{K}^0\rangle \right), \quad |K_2\rangle = \frac{1}{\sqrt{2}} \left(|K^0\rangle + |\bar{K}^0\rangle \right), \quad (2.2)$$

where the former has $CP = +1$ and the latter $CP = -1$. However, CP is mildly violated by weak interactions and therefore the mass eigenstates $|K_S\rangle$ and $|K_L\rangle$, characterized by definite lifetimes, are different from $|K_1\rangle$ and $|K_2\rangle$:

$$|K_S\rangle = \frac{|K_1\rangle + \varepsilon|K_2\rangle}{\sqrt{1 + |\varepsilon|^2}}, \quad |K_L\rangle = \frac{|K_2\rangle + \varepsilon|K_1\rangle}{\sqrt{1 + |\varepsilon|^2}}, \quad (2.3)$$

¹Leptonic and semi-leptonic decays of kaons in the minimal “3+1” case have been studied in detail in Ref. [33]. For a systematic study of $K \rightarrow \pi\nu\bar{\nu}$ in the LEFT (without right-handed neutrinos), see Ref. [34].

LNC operators			LNV operators		
Name	Structure	N_{pars}	Name	Structure	N_{pars}
$\mathcal{O}_{dN}^{V,RR}$	$(\bar{d}_R \gamma_\mu d_R) (\bar{N}_R \gamma^\mu N_R)$	9	$\mathcal{O}_{dN}^{S,RR}$	$(\bar{d}_L d_R) (\bar{N}_R^c N_R)$	18
$\mathcal{O}_{uN}^{V,RR}$	$(\bar{u}_R \gamma_\mu u_R) (\bar{N}_R \gamma^\mu N_R)$	4	$\mathcal{O}_{uN}^{S,RR}$	$(\bar{u}_L u_R) (\bar{N}_R^c N_R)$	8
$\mathcal{O}_{dN}^{V,LR}$	$(\bar{d}_L \gamma_\mu d_L) (\bar{N}_R \gamma^\mu N_R)$	9	$\mathcal{O}_{dN}^{S,LR}$	$(\bar{d}_R d_L) (\bar{N}_R^c N_R)$	18
$\mathcal{O}_{uN}^{V,LR}$	$(\bar{u}_L \gamma_\mu u_L) (\bar{N}_R \gamma^\mu N_R)$	4	$\mathcal{O}_{uN}^{S,LR}$	$(\bar{u}_R u_L) (\bar{N}_R^c N_R)$	8

Table 1. Four-fermion operators in N_R LEFT, involving two quarks and two N_R 's, assuming one generation of N_R . LNV operator structures require “+h.c.”. In the third column, we provide the number of independent real parameters, N_{pars} , associated with each operator structure.

LNC operators		LNV operators	
Name	Structure	Name	Structure
$\mathcal{O}_{udeN}^{V,RR}$	$(\bar{u}_R \gamma_\mu d_R) (\bar{e}_R \gamma^\mu N_R)$	$\mathcal{O}_{udeN}^{V,LL}$	$(\bar{u}_L \gamma_\mu d_L) (\bar{e}_L \gamma^\mu N_R^c)$
$\mathcal{O}_{udeN}^{V,LR}$	$(\bar{u}_L \gamma_\mu d_L) (\bar{e}_R \gamma^\mu N_R)$	$\mathcal{O}_{udeN}^{V,RL}$	$(\bar{u}_R \gamma_\mu d_R) (\bar{e}_L \gamma^\mu N_R^c)$
$\mathcal{O}_{udeN}^{S,RR}$	$(\bar{u}_L d_R) (\bar{e}_L N_R)$	$\mathcal{O}_{udeN}^{S,LL}$	$(\bar{u}_R d_L) (\bar{e}_R N_R^c)$
$\mathcal{O}_{udeN}^{T,RR}$	$(\bar{u}_L \sigma_{\mu\nu} d_R) (\bar{e}_L \sigma^{\mu\nu} N_R)$	$\mathcal{O}_{udeN}^{T,LL}$	$(\bar{u}_R \sigma_{\mu\nu} d_L) (\bar{e}_R \sigma^{\mu\nu} N_R^c)$
$\mathcal{O}_{udeN}^{S,LR}$	$(\bar{u}_R d_L) (\bar{e}_L N_R)$	$\mathcal{O}_{udeN}^{S,RL}$	$(\bar{u}_L d_R) (\bar{e}_R N_R^c)$

Table 2. Four-fermion operators in N_R LEFT, involving two quarks, one charged lepton, and one N_R . Both LNC and LNV operator structures require “+h.c.”. For one generation of N_R , there are 36 independent real parameters associated with each operator structure.

where ε is the parameter accounting for indirect CP violation in neutral kaon decays. K_S (K_L) denotes the neutral kaon with the shorter (longer) lifetime. Experimentally, $|\varepsilon| \approx 2.23 \times 10^{-3}$ [38], and for the purposes of this work we can safely neglect it. Thus, in what follows we assume $|K_S\rangle \approx |K_1\rangle$ and $|K_L\rangle \approx |K_2\rangle$.

2.2 Effective field theory with right-handed neutrinos

We will work in the framework of the low-energy effective field theory extended with right-handed neutrinos, N_R , dubbed as N_R LEFT, see *e.g.* [27–30]. We assume N_R to be a Majorana particle and allow for both lepton-number-conserving (LNC) and lepton-number-violating (LNV) operators. Charm and bottom meson decays triggered by four-fermion effective operators with N_R have been studied in detail in Refs. [23, 24]. Here, we are interested in the decays of kaons induced by four-fermion interactions. These interactions can be grouped into pair- N_R operators given in table 1 and single- N_R operators provided in table 2.² Since the top quark is not in the spectrum of the N_R LEFT, we have $n_u = 2$

²In what follows, we will not consider single- N_R operators with an active neutrino ν_L .

Decay	Branching ratio	Decay	Branching ratio
$K_L \rightarrow \pi^0 \nu \bar{\nu}$	$< 3.0 \times 10^{-9}$ at 90% C.L.	$K^+ \rightarrow e^+ \nu_e$	$(1.582 \pm 0.007) \times 10^{-5}$
$K^+ \rightarrow \pi^+ \nu \bar{\nu}$	$(1.14_{-0.33}^{+0.40}) \times 10^{-10}$	$K^+ \rightarrow \pi^0 e^+ \nu_e$	$(5.07 \pm 0.04) \times 10^{-2}$
		$K_S \rightarrow \pi^\pm e^\mp \nu_e$	$(7.04 \pm 0.08) \times 10^{-4}$
		$K_L \rightarrow \pi^\pm e^\mp \nu_e$	$(40.55 \pm 0.11) \times 10^{-2}$

Table 3. Branching ratios of semi-invisible kaon decays [38]. For $K_{S/L} \rightarrow \pi^\pm e^\mp \nu_e$, the values are for the sum of particle and antiparticle states indicated.

and $n_d = n_e = n_\nu = 3$, with n_f denoting the number of generations of a fermion f . In addition, we assume one generation of N_R .

Generically, N_R mixes with the active neutrinos at the renormalizable level. Integrating out the W boson leads to the following contribution to the effective Lagrangian:

$$\mathcal{L}_{\text{mix}} = -\frac{4G_F}{\sqrt{2}} V_{ij} U_{\ell N} (\overline{u_{iL}} \gamma_\mu d_{jL}) (\overline{e_{\ell L}} \gamma^\mu N_R^c) + \text{h.c.}, \quad (2.4)$$

where G_F is the Fermi constant, V is the CKM quark mixing matrix, and $U_{\ell N}$ is active-heavy neutrino mixing. For charged kaon decays, the relevant CKM matrix element is V_{us} . In what follows, we will separate this contribution from the corresponding operator in table 2 by denoting its Wilson coefficient (WC) as

$$c_{\text{mix}} = -\frac{4G_F}{\sqrt{2}} V_{us} U_{\ell N}, \quad \text{with} \quad |c_{\text{mix}}| \approx \frac{0.45 |U_{\ell N}|}{v^2}. \quad (2.5)$$

For a more detailed discussion of N_R LEFT, including the running of the considered operators and their matching to the N_R SMEFT operators, see Ref. [24].

2.3 HNL production in kaon decays

The pair- N_R operators \mathcal{O}_{dN} from table 1 involving d and s quarks trigger the following two- and three-body decays: $K_{S/L} \rightarrow NN$, $K_{S/L} \rightarrow \pi^0 NN$ and $K^\pm \rightarrow \pi^\pm NN$. The single- N_R operators \mathcal{O}_{udeN} from table 2 containing u and s quarks induce $K^\pm \rightarrow e^\pm N$, $K^\pm \rightarrow \pi^0 e^\pm N$ and $K_{S/L} \rightarrow \pi^\pm e^\mp N$. In appendix A, we provide the formulae for the two-body decay widths and the three-body decay amplitudes. The three-body decay widths are then computed according to the procedure explained in Refs. [23, 24].

If the products of HNL decays are not detected, the kaon decay modes we are interested in contribute to $K_{S/L} \rightarrow \text{inv.}$, $K_{S/L} \rightarrow \pi^0 \nu \bar{\nu}$, $K^\pm \rightarrow \pi^\pm \nu \bar{\nu}$, and $K^+ \rightarrow e^+ \nu_e$, $K^+ \rightarrow \pi^0 e^+ \nu_e$, $K_{S/L} \rightarrow \pi^\pm e^\mp \nu_e$. The branching ratios of the decays into final states with at least one charged particle have been measured, whereas for $K_L \rightarrow \pi^0 \nu \bar{\nu}$ a stringent upper limit on the branching ratio has been obtained. We summarize the current experimental results in table 3. We will take them into account when deriving the limits on the WCs of the pair- N_R and single- N_R operators. In the case of a measured branching ratio, we will require the

new contribution not to exceed twice the experimental error, whereas for $K_L \rightarrow \pi^0 NN$, we will demand that its branching ratio is smaller than 3.0×10^{-9} in accordance with the current upper bound on the branching ratio of $K_L \rightarrow \pi^0 \nu \bar{\nu}$ [38].

In figure 1, we display the branching ratios of kaon decays triggered by the LNC operator $\mathcal{O}_{dN,21}^{V,RR}$ and by the LNV operator $\mathcal{O}_{dN,21}^{S,RR}$. In each case, we assume that the corresponding WC is either real (left panel) or purely imaginary (right panel). For the LNC operator, a real (purely imaginary) WC does not allow for $K_S \rightarrow NN$ and $K_L \rightarrow \pi^0 NN$ ($K_L \rightarrow NN$ and $K_S \rightarrow \pi^0 NN$), as can be inferred from eqs. (A.15) and (A.22) (eqs. (A.16) and (A.21)).³ For small m_N , the allowed two-body decay is suppressed, since the corresponding decay width scales with m_N^2 , see eqs. (A.15) and (A.16). In this figure, we fix the absolute value of the operator coefficient to $10^{-6} v^{-2}$ in order to comply with the measurements reported in the left panel of table 3, in particular, with that of $K^+ \rightarrow \pi^+ \nu \bar{\nu}$. Switching on $\mathcal{O}_{dN,21}^{V,LR}$ and $\mathcal{O}_{dN,21}^{S,LR}$ (one at a time) would lead to the same results as for $\mathcal{O}_{dN,21}^{V,RR}$ and $\mathcal{O}_{dN,21}^{S,RR}$, respectively.

In figure 2, we plot the branching ratios of kaon decays induced by the LNC operators $\mathcal{O}_{udeN,12}^{V,RR}$, $\mathcal{O}_{udeN,12}^{S,RR}$, and $\mathcal{O}_{udeN,12}^{T,RR}$, with respective WC $c_{\mathcal{O}}$, as well as by active-heavy neutrino mixing U_{eN} . We show three representative cases: (i) $U_{eN} = 10^{-5}$ and $c_{\mathcal{O}} = 0$, (ii) $U_{eN} = 0$ and $c_{\mathcal{O}} = 10^{-5} v^{-2}$, and (iii) $U_{eN} = 10^{-5}$ and $c_{\mathcal{O}} = 10^{-5} v^{-2}$. The value of the operator coefficient ensures that the branching ratios are compatible with the errors in the measurements presented in the right panel of table 3, most importantly, with that of $K^+ \rightarrow e^+ \nu_e$. The value $U_{eN} = 10^{-5}$ ($|U_{eN}|^2 = 10^{-10}$) is such that it is below the existing constraints. For HNLs lighter than the kaons, the leading constraints on the mixing parameter come from NA62 [39], PS191 [40], and T2K [41], which set upper limits at the level of $|U_{eN}|^2 \sim 5 \times 10^{-10}$. For even lighter HNLs, below the pion mass, PIENU [42] has ruled out parameter space corresponding to $|U_{eN}|^2 > 10^{-7} \sim 10^{-8}$. Moreover, with the chosen value for the mixing, its contribution is comparable to the contributions of most operators for $c_{\mathcal{O}} \sim 10^{-5} v^{-2}$, cf. eq. (2.5). For the scalar operator $\mathcal{O}_{udeN,12}^{S,RR}$, the constraints from NA62 set limits on the operator to $c_{\mathcal{O}} \sim 10^{-6} v^{-2}$.

In figure 3, we show the branching ratios for the same processes as in figure 2, but for the LNV operators $\mathcal{O}_{udeN,12}^{V,RL}$, $\mathcal{O}_{udeN,12}^{S,RL}$, and $\mathcal{O}_{udeN,12}^{T,LL}$. In the absence of mixing, the results are identical to those for the corresponding LNC operators (switched on one at a time). In the presence of mixing, there is an interference between the effective operator generated by new physics and the four-fermion interaction (see eq. (2.4)) arising from integrating out the W boson. Its effect is more pronounced for the vector-type operators, and it is stronger for the LNV operator, as can be understood from eq. (A.17).

3 Experiments and simulation

A whole list of far detectors has been proposed for operation in the vicinity of various interaction points of the LHC, either during Run 3 or the HL-LHC phase; some of them

³We note that this is strictly true only in the limit $\varepsilon \rightarrow 0$.

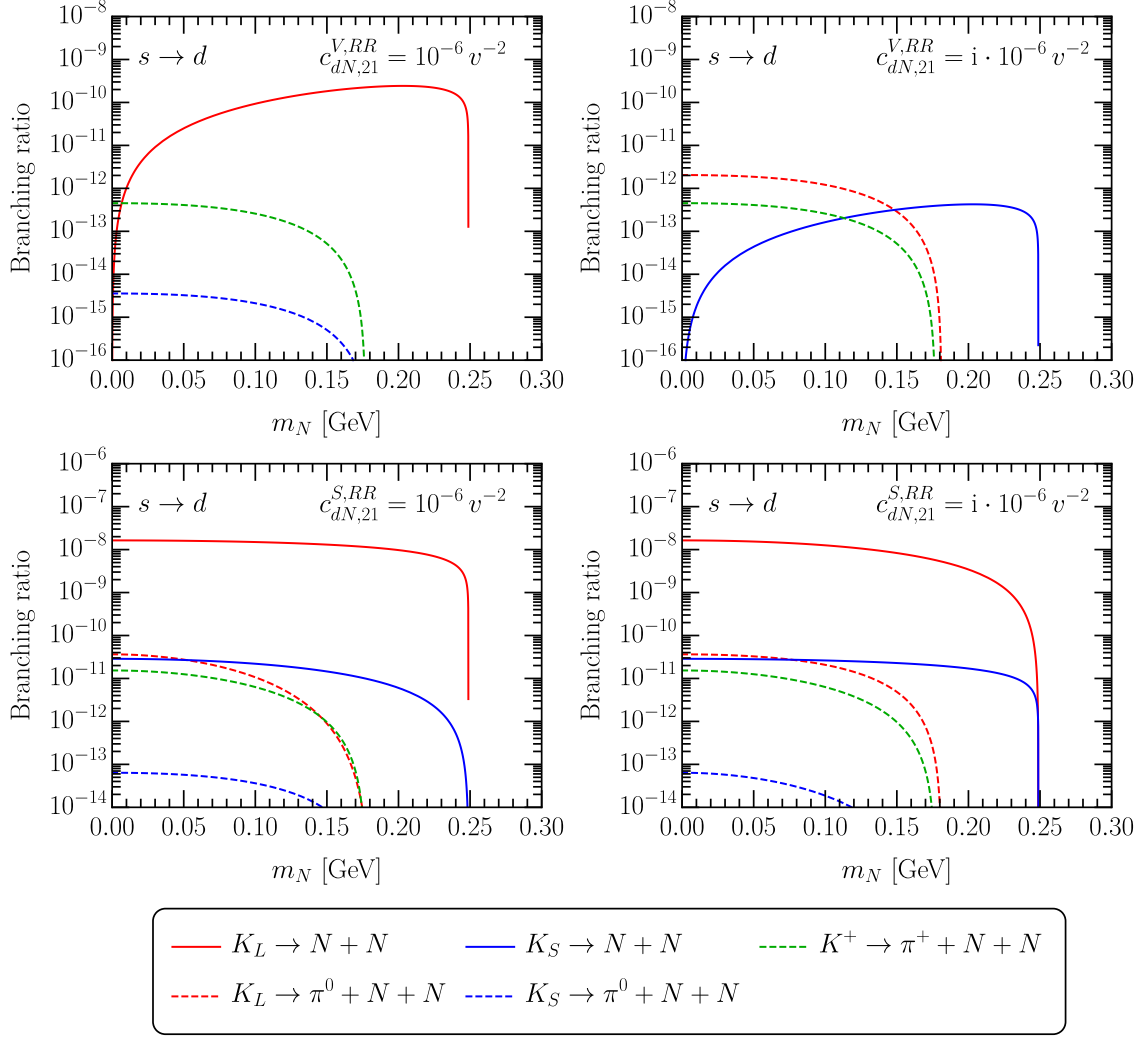


Figure 1. Branching ratios of kaon decays triggered by the LNC (top) and LNV (bottom) pair- N_R operators. In the left (right) panel, the corresponding WC is purely real (imaginary).

have even been approved and are running, including FASER and MoEDAL-MAPP1. Since they are all sensitive to signatures of tracks stemming from displaced decays of LLPs taking place inside their fiducial volumes, we will perform the numerical analysis taking into account these proposals comprehensively.

We classify these detectors according to their associated IP at the LHC. For the ATLAS IP, ANUBIS [8], FASER [4, 5], and FASER2 [3] are relevant. ANUBIS⁴ is a detector proposed to be installed inside one of the service shaft above the ATLAS IP. It has a cylindrical shape of 56 m height and 18 m diameter. Being close to the ATLAS IP, it is

⁴Very recently, a new design of ANUBIS has been discussed [43, 44]. Instead of being placed inside one of the service shafts, ANUBIS is now considered to be installed at the ATLAS cavern ceiling or shaft bottom. Given the changing status of the proposal, we stick to the original design for sensitivity study as a good reference for interested readers.

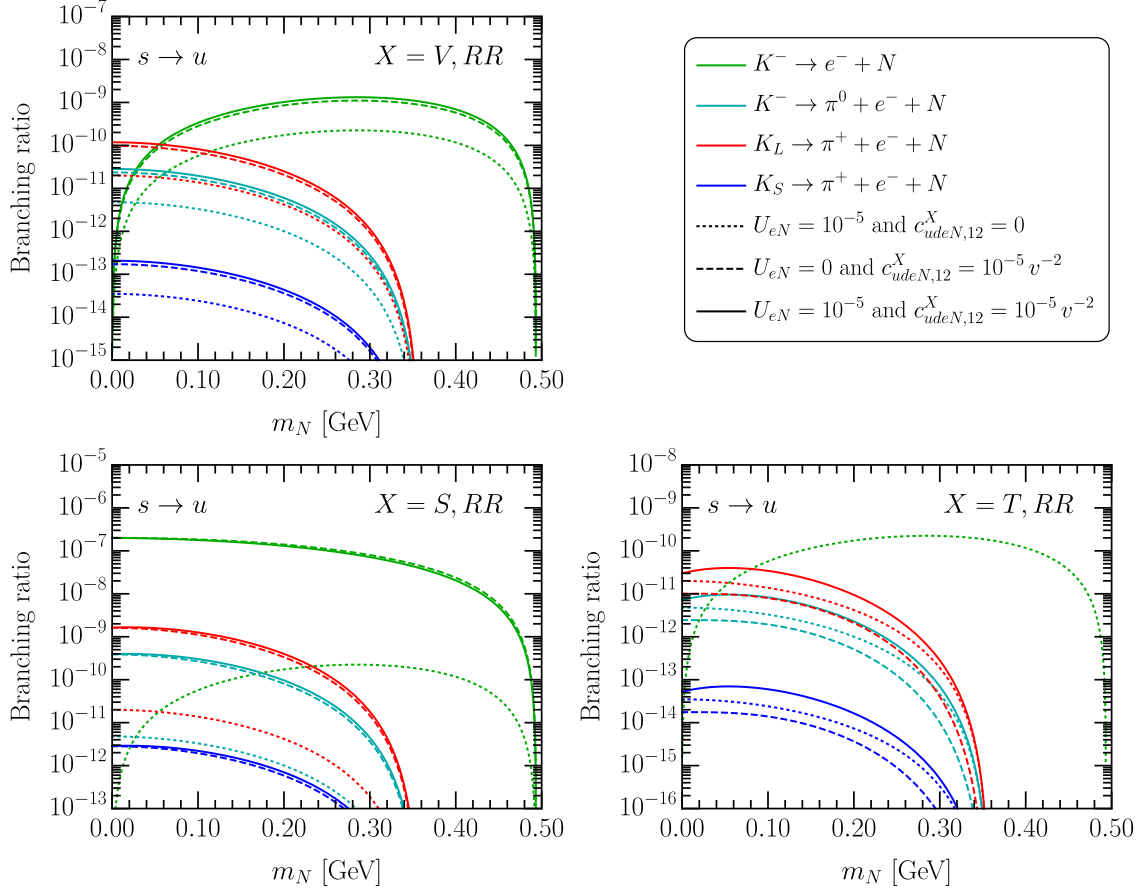


Figure 2. Branching ratios of kaon decays triggered by the LNC single- N_R operators with electron, as well as by active-heavy mixing U_{eN} .

expected to suffer from certain background sources such as neutral kaons. Nevertheless, exclusion bounds at 95% confidence level (C.L.) are usually shown with 3 signal events, assuming zero background, and we will follow the practice in this paper. FASER is currently collecting data at the LHC; first results can be found in Refs. [45, 46]. It is a small cylindrical detector installed in the very forward position along the beam direction, with a distance of 480 m from the interaction point. Further, an upgraded program of FASER, FASER2, has been suggested to be built at the site of the proposed Forward Physics Facility [3]. It is larger than FASER and has hence better acceptances to LLPs. ANUBIS and FASER2 should collect in total 3 ab^{-1} integrated luminosity data, while FASER will have order of 150 fb^{-1} integrated luminosity.

Near the CMS IP, MATHUSLA [1, 11, 12] and FACET [10] have been proposed. MATHUSLA would be an experiment on the ground, with about 100 m distance from the CMS IP. It would have a huge effective volume of $100 \text{ m} \times 100 \text{ m} \times 25 \text{ m}$. FACET is suggested to be a sub-system of the CMS experiment; with a cylindrical shape, it has a distance of 101 m from the CMS IP, enclosing the beam pipe. Moreover, with a radius

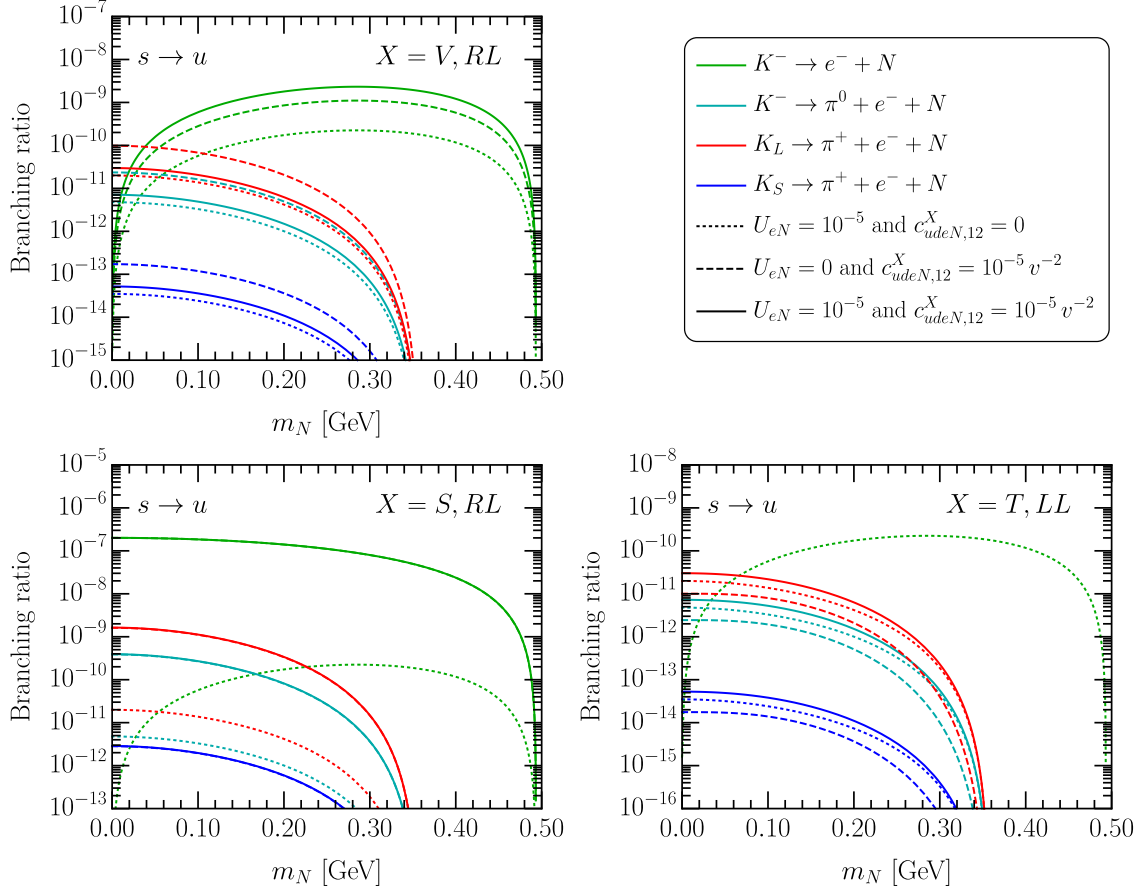


Figure 3. Branching ratios of kaon decays triggered by the LNV single- N_R operators with electron, as well as by active-heavy mixing U_{eN} .

of 0.5 m and a length of 18 m, FACET is relatively large compared to FASER. Both MATHUSLA and FACET would be running during the HL-LHC and will hence have an integrated luminosity of 3 ab^{-1} .

Finally, for the LHCb IP, we have CODEX-b [9], and MoEDAL-MAPP1 and MoEDAL-MAPP2 [6, 7]. CODEX-b has been proposed as a cubic box with a dimension of $10 \text{ m} \times 10 \text{ m} \times 10 \text{ m}$ covering the pseudorapidity range $[0.2, 0.6]$, roughly 10 m away from IP8. MoEDAL-MAPP1 is a small detector of about 140 m^3 in a gallery of negative pseudorapidity with respect to the LHCb IP, under operation during Run 3, and MoEDAL-MAPP2 is an enlarged version of MAPP1, to be running during the HL-LHC period. The integrated luminosity associated with the LHCb interaction point is lower compared to that of ATLAS or CMS. CODEX-b and MoEDAL-MAPP2 will have an integrated luminosity of 300 fb^{-1} while MoEDAL-MAPP1 has only 30 fb^{-1} .

For a more detailed summary of these proposals, we refer the reader to *e.g.* Refs. [2, 23, 47], as well as to the respective references proposing the detectors.

In order to obtain the kinematics of the HNLs produced from kaons, we make use of the

tool Pythia8 with the module *SoftQCD:all*. The kaons are generated in pp collisions with a center-of-mass-energy 14 TeV, and are set to decay exclusively in the signal-event channels. Pythia8 provides the boost factor and the polar angle of each simulated HNL. We note that since kaons are themselves long-lived, we let Pythia8 decide the decay positions of the kaons and thus take into account the production position of the HNL (= the decay position of the kaon) as well as the polar angle and boost factor of the HNL, in the computation of the HNLs' average decay probability inside the far detectors. The total signal-event rates at each detector can be computed with the following formula

$$N_S = \sum_{K's} N_K \cdot n \cdot \text{BR}(K \rightarrow n N + \text{anything}) \cdot \epsilon \cdot \text{BR}(N \rightarrow \text{visible}) , \quad (3.1)$$

where the summation goes over different kaons, N_K is the total number of kaons, $n = 1, 2$ is the number of HNLs produced in the considered kaon decays, $\text{BR}(N \rightarrow \text{visible})$ is the visible decay branching ratio of the HNL, and ϵ is the average decay probability in a far detector. We estimate the number of kaons N_K , with the help of the tool EPOS LHC [48] provided in the CRMC simulation package [49], to be $N_{K^\pm} = 2.38 \times 10^{18}$, $N_{K_S} = 1.31 \times 10^{18}$, and $N_{K_L} = 1.30 \times 10^{18}$, over the whole 4π solid angle. The computation procedure of ϵ is based on the exact formulae given in Refs. [23, 24, 50–52] and the further development presented in Ref. [53] for LLPs from kaons. As the kaons, especially K^\pm and K_L , travel macroscopic distances, the infrastructure surrounding the IPs may affect the kinematics of the kaons. To simplify the analysis, we neglect the influence of any magnetic fields present at the IP. Additionally, we introduce cut-offs for the production positions of the HNL that are included in the signal-event rates N_S , resulting in conservative estimates. Here, we provide a brief summary of the cut-offs we employ in our simulation; for more detail, see Ref. [53]. For example, a lead shield covering the total fiducial volume in order to veto neutral background events is placed approximately 5 m in front of CODEX-b. Hence, we require the kaons to decay before reaching the shield. For detectors in the far forward region (FASER, FASER2, and FACET), we employ the beamline geometry of the ATLAS and CMS IP, which involve absorbers for charged and neutral particles in order to protect beamline infrastructure. The hadron calorimetry of ATLAS and CMS restricts the decay region of the kaons for ANUBIS and MATHUSLA, respectively. Lastly, for MoEDAL-MAPP1 and MAPP2, the natural rock between the IP and the detectors is the limiting factor. Hence, the kaons are required to decay within the 3.8 m wide beam cavern.

Finally, we discuss the procedure we apply for recasting the bounds on the HNLs in the minimal scenario, obtained in some past searches, into those on the HNLs in the EFT scenarios considered here. In general, we follow the approaches laid out in Refs. [36, 54, 55] (see also Ref. [56]). We consider three searches at NA62 [39], PS191 [40], and T2K [41]. Since these searches all require a prompt charged lepton, they are applicable only to the single- N_R scenarios. We first consider the NA62 search, which looked for HNL production in K^+ decays to positrons and missing energy, assuming the proper lifetime of N is larger than 50 ns. The search obtained bounds on $\text{BR}(K^+ \rightarrow e^+ N)$ and hence those on the

Benchmark	Production	Decay	Benchmark	Production	Decay
B1.1	$c_{dN,21}^{V,RR} \in \mathbb{R}$	U_{eN}	B3	$c_{udeN,12}^{V,RR}$	$c_{udeN,11}^{V,RR}$
B1.2	$c_{dN,21}^{V,RR} \in i\mathbb{R}$	U_{eN}	B4	$c_{udeN,12}^{S,RR}$	$c_{udeN,11}^{S,RR}$
B2.1	$c_{dN,21}^{S,RR} \in \mathbb{R}$	U_{eN}	B5	$c_{udeN,12}^{V,RR}$ and U_{eN}	U_{eN}
B2.2	$c_{dN,21}^{S,RR} \in i\mathbb{R}$	U_{eN}	B6	$c_{udeN,12}^{S,RR}$ and U_{eN}	U_{eN}
			B7	$c_{udeN,12}^{V,RL}$ and U_{eN}	U_{eN}
			B8	$c_{udeN,12}^{S,RL}$ and U_{eN}	U_{eN}

Table 4. Benchmarks for the scenarios with pair- N_R (left) and single- N_R (right) operators.

active-sterile neutrino mixing, as functions of the sterile neutrino mass. We simply convert $\text{BR}(K^+ \rightarrow e^+N)$ to the production Wilson coefficient of the single- N_R scenario in question, for each mass value, and obtain the corresponding recast bounds. Both the PS191 and T2K searches are for both a prompt charged lepton and a displaced vertex at the detached detector. For PS191, we extract the sensitivity curve presented in the plane $|U_{eN}|^2$ vs. m_N for the signal process $K^+ \rightarrow e^+N$, $N \rightarrow e^-\pi^+$ and its charge-conjugate channel, and for the T2K near detector ND280, the signal process $K^\pm \rightarrow e^\pm N$, $N \rightarrow e^\pm\pi^\mp$ is considered. By rescaling the production and visible decay rates, we obtain the recast bounds in the EFT parameter space.

4 Results

For presenting the numerical results, we choose several benchmarks characterized by the different couplings responsible for the HNL production and decay. We summarize them in table 4. In total, we consider four scenarios with pair- N_R operators (benchmarks B1 and B2, each having two sub-cases) and six scenarios with single- N_R operators (benchmarks B3–B8).

For benchmark B1 (B2), HNL production is governed by the LNC (LNV) pair- N_R operator $\mathcal{O}_{dN,21}^{V,RR}$ ($\mathcal{O}_{dN,21}^{S,RR}$), while HNL decay proceeds via active-heavy neutrino mixing U_{eN} . For each of these two operators, we consider two cases: (i) real WC and (ii) purely imaginary WC, *cf.* figure 1 and the related discussion. First, in figure 4, we fix the absolute value of the WC to $10^{-6}v^{-2}$ (to respect the constraint coming from $K^+ \rightarrow \pi^+\nu\bar{\nu}$) and display the projected exclusion limits in the plane $|U_{eN}|^2$ vs. m_N for three signal events. The curves correspond to 95% C.L. limits (under the assumption of zero background). For the LNC operator, the sensitivities are approximately two orders of magnitude weaker in the case of purely imaginary WC (B1.2, top-right plot) than in the case of real WC of the same size (B1.1, top-left plot). This can be understood from figure 1, which shows that for the same size of the WC, $\text{BR}(K_S \rightarrow NN)$ is about two orders of magnitude smaller than $\text{BR}(K_L \rightarrow NN)$, whereas the production numbers of K_S and K_L are nearly the same. The difference in the sensitivities is much milder for the LNV operator, for which the branching

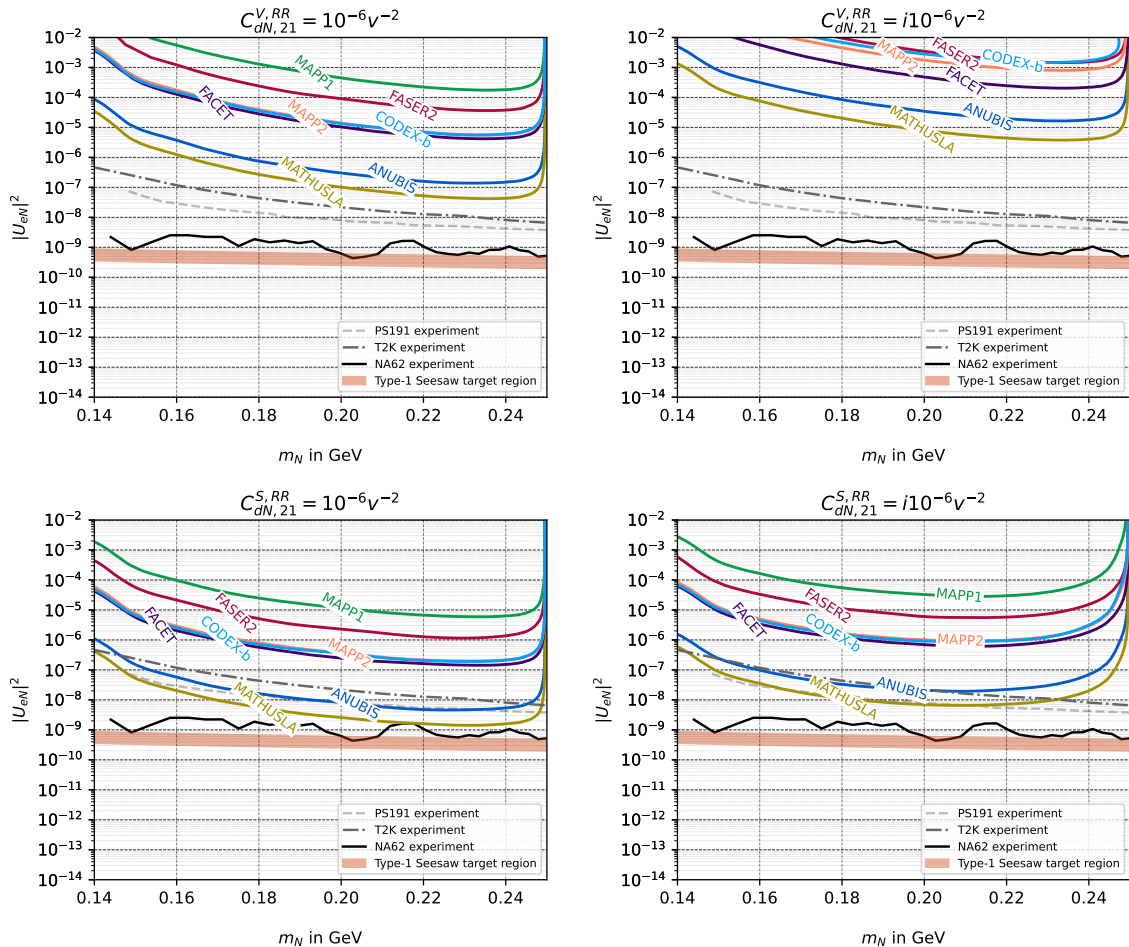


Figure 4. Projected exclusion limits in the plane $|U_{eN}|^2$ vs. m_N for pair- N_R operator benchmarks B1.1 and B1.2 (top), and B2.1 and B2.2 (bottom). The absolute value of the corresponding WC has been fixed to $10^{-6}v^{-2}$. The current bounds from NA62, T2K, and PS191, as well as the type-I seesaw target region where $m_\nu = 0.05\text{--}0.12$ eV, are also shown.

ratios of the relevant kaon decays differ only slightly between the cases of real and purely imaginary WC.

Among the considered LLP detectors, the best limit comes from MATHUSLA, which can probe $|U_{eN}|^2$ down to 4×10^{-8} (1.4×10^{-9}) at $m_N \approx 0.23$ GeV for B1.1 (B2.1). It is followed by ANUBIS, which has a factor of a few weaker sensitivity. MAPP2, FACET and CODEX-b provide very similar exclusion limits, which are approximately two orders of magnitude weaker than the expected limits from MATHUSLA. Finally, FASER2 and MAPP1 have the weakest depicted sensitivities.⁵ We also show the existing limits on active-heavy neutrino mixing obtained by the NA62 [39], T2K [41], and PS191 [40] experiments.

⁵For FASER, there is no isocurve shown in figure 4 and figure 5. Because of the small geometric acceptance and comparatively lower integrated luminosity, the simulated number of signal events is less than three in the shown parameter region.

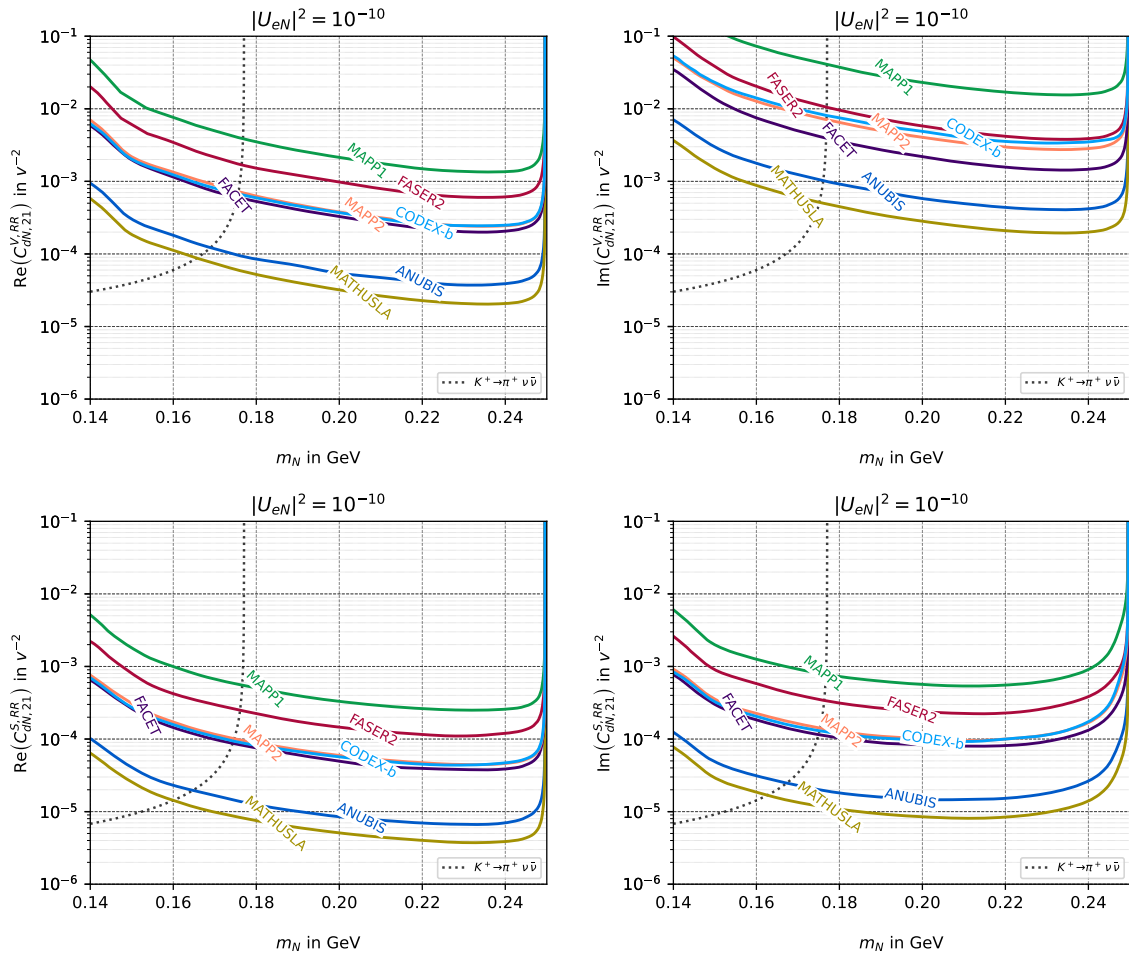


Figure 5. Exclusion limits in the plane WC vs. m_N for pair- N_R operator benchmarks B1.1 and B1.2 (top), and B2.1 and B2.2 (bottom). The active-heavy neutrino mixing parameter has been fixed as $|U_{eN}|^2 = 10^{-10}$. The dotted line represents the constraint originating from the measured branching ratio of $K^+ \rightarrow \pi^+ \nu \bar{\nu}$.

Though derived under the hypothesis of the minimal mixing case, these limits apply to the considered EFT scenarios as well. As can be seen, NA62 outperforms all the far detectors and already touches the (naive) type-I seesaw band, where the values of m_N and U_{eN} yield the light neutrino mass $m_\nu = 0.05\text{--}0.12$ eV.

In figure 5, we fix $|U_{eN}|^2 = 10^{-10}$ and show the exclusion limits in the plane WC vs. m_N . For benchmark B1.1 (B1.2), MATHUSLA will be able to probe the WC as small as $2 \times 10^{-5} v^{-2}$ ($2 \times 10^{-4} v^{-2}$) for m_N in the range 0.22–0.24 GeV. These numbers translate

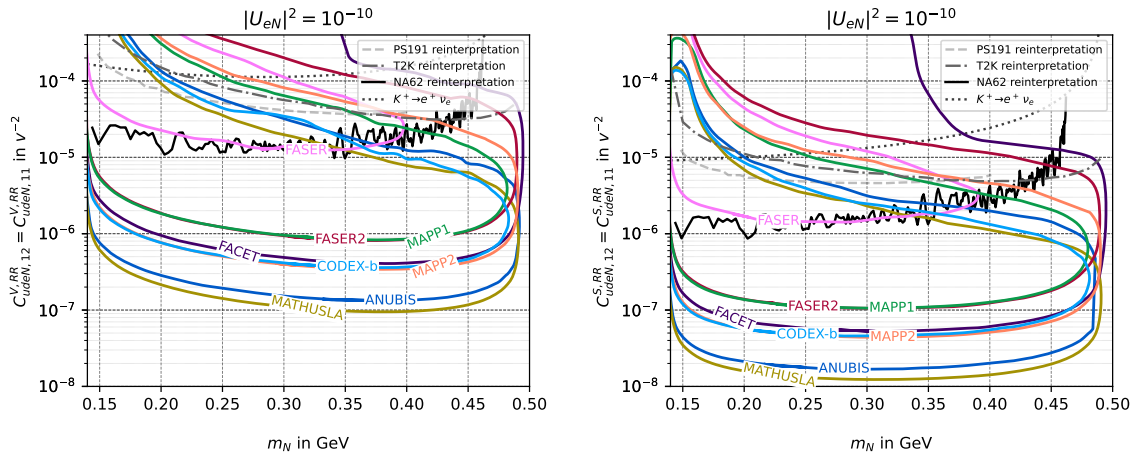


Figure 6. Exclusion limits in the plane WC vs. m_N for single- N_R operator benchmarks B3 (left) and B4 (right). The production and decay couplings have been assumed to be equal. The recast bounds from NA62, T2K, and PS191, as well as the constraint originating from the measured branching ratio of $K^+ \rightarrow e^+ \nu_e$, are also shown.

to the new physics scale Λ of 55 (17) TeV.⁶ In the case of the LNV operator, we find that for benchmark B2.1 (B2.2), MATHUSLA can exclude the effective couplings down to $4 \times 10^{-6} v^{-2}$ for $m_N \approx 0.23$ GeV (8×10^{-6} for $m_N \approx 0.21$ GeV). However, being an LNV operator, it originates at dimension 7 in the N_R SMEFT, and hence, these exclusion limits translate to Λ of around 11 (9) TeV. We also show the constraint originating from the measurement of the branching ratio of $K^+ \rightarrow \pi^+ \nu \bar{\nu}$. It is complementary to the projected limits for $m_N \lesssim 0.16$ – 0.17 GeV.

Next, we consider the single- N_R operator benchmarks summarized in the right part of table 4. We start with benchmarks B3 and B4, for which we assume that both HNL production and decay proceed via the same effective operator, but carrying different quark flavor indices. The indices 12 lead to the HNL production in kaon decays, while the indices 11 realize the decay $N \rightarrow e^\mp \pi^\pm$. For these benchmarks, we also assume that there is no active-heavy neutrino mixing. We consider two single- N_R operators $\mathcal{O}_{udeN}^{V,RR}$ and $\mathcal{O}_{udeN}^{S,RR}$, both conserving the lepton number. (The results for the corresponding LNV operators are the same under the assumption of zero active-heavy neutrino mixing.) For graphical presentation, we choose to set the production and decay couplings equal, *i.e.* $c_{udeN,12}^{V,RR} = c_{udeN,11}^{V,RR}$ for B3, and $c_{udeN,12}^{S,RR} = c_{udeN,11}^{S,RR}$ for B4, and show the derived exclusion limits in the plane WC vs. m_N , see figure 6. In addition to the sensitivities of the proposed LLP detectors at the LHC, we show the recast bounds from NA62 [39], T2K [41], and PS191 [40]

⁶We associate the new physics scale Λ with the effective operators in the N_R SMEFT, assuming their WCs are Λ^{4-d} , with d denoting the operator mass dimension. The LNC four-fermion operators in the N_R LEFT arise from $d = 6$ four-fermion operators in the N_R SMEFT, whereas the LNV four-fermion operators in the N_R LEFT originate from $d = 7$ operators in the N_R SMEFT. For details of the matching between the two effective theories, see *e.g.* Refs. [23, 24].

obtained according to the procedure explained at the end of Sec. 3. Except for FASER, of which the sensitivity is comparable to that of NA62, all the far detectors at the LHC will have better reach to these scenarios than NA62, which excludes WC values larger than approximately $(1-2)\times 10^{-5}v^{-2}$ ($(9-20)\times 10^{-7}v^{-2}$) for benchmark B3 (B4). For the vector-type operator and $m_N \approx 0.35-0.40$ GeV, MATHUSLA will probe the effective couplings as small as $9.5 \times 10^{-8}v^{-2}$, and FASER down to $1.4 \times 10^{-5}v^{-2}$, with the sensitivities of the other experiments lying between these two extremes. Translating these numbers to the new-physics scale Λ , we find that MATHUSLA (FASER) will be sensitive to Λ as high as 798 (65) TeV. For the scalar-type operator, the reach in the N_R LEFT WC is around one order of magnitude better, owing to the larger branching ratio of $K^\pm \rightarrow e^\pm N$ in this case, see figure 2. The new-physics scales, which could be probed by MATHUSLA (FASER) for $m_N \approx 0.25-0.35$ GeV, are in excess of 2000 (200) TeV.

Finally, we turn to benchmarks B5–B8, where both an effective operator and active-heavy neutrino mixing contribute to HNL production, while the HNL decay proceeds via mixing only, see table 4. Here, we consider both LNC vector (B5) and scalar (B6) operators, and LNV vector (B7) and scalar (B8) operators, since the interference between the effective interaction and the mixing term is slightly different in the LNC and LNV cases, *cf.* figures 2 and 3. In figure 7, we fix the corresponding WC to either $10^{-5}v^{-2}$ for vector operators (to satisfy the constraint coming from $K^+ \rightarrow e^+\nu_e$), or $10^{-6}v^{-2}$ for scalar operators (to satisfy recast bounds from NA62) and present the sensitivities in the plane $|U_{eN}|^2$ vs. m_N . For the vector-type operators and $m_N \approx 0.35-0.40$ GeV, MATHUSLA could probe $|U_{eN}|^2$ down to 3.0 (2.0) $\times 10^{-10}$ for the LNC (LNV) operator. For the scalar-type operators in the same m_N -range, the MATHUSLA reach is $|U_{eN}|^2 \approx 9.0$ (4.0) $\times 10^{-9}$ for the LNC (LNV) operator.

We also display the recast bounds from NA62, T2K, and PS191. The NA62 limit is more stringent than the expected limits from the future LLP detectors for $m_N \lesssim 0.35$ (0.41) GeV in B5 and B8 (B6 and B7). For larger m_N , MATHUSLA takes over, excluding new parts of the parameter space. In particular, for B7, the projected MATHUSLA exclusion limits can probe the seesaw target region for 0.25 GeV $\lesssim m_N \lesssim 0.45$ GeV.

In figure 8, we fix $|U_{eN}|^2 = 10^{-10}$ and show the exclusion limits in the plane WC vs. m_N . We again depict recast bounds from NA62, T2K, and PS191. The recast NA62 bound covers the ranges which will be accessible to the future LLP detectors for $m_N \lesssim 0.45$ GeV. For larger HNL masses, MATHUSLA will probe an unexplored region of the parameter space, ruling out the WC $\gtrsim 2 \times 10^{-5}v^{-2}$ ($\gtrsim 3 \times 10^{-6}v^{-2}$) for the vector-type (scalar-type) operators. We further see, that the NA62 constraints for B6 and B8 exclude WC $\gtrsim 10^{-6}v^{-2}$, justifying the WC choice in figure 7. Overall, for benchmarks B5–B8, the future far detectors will access new parameter space for larger HNL masses.

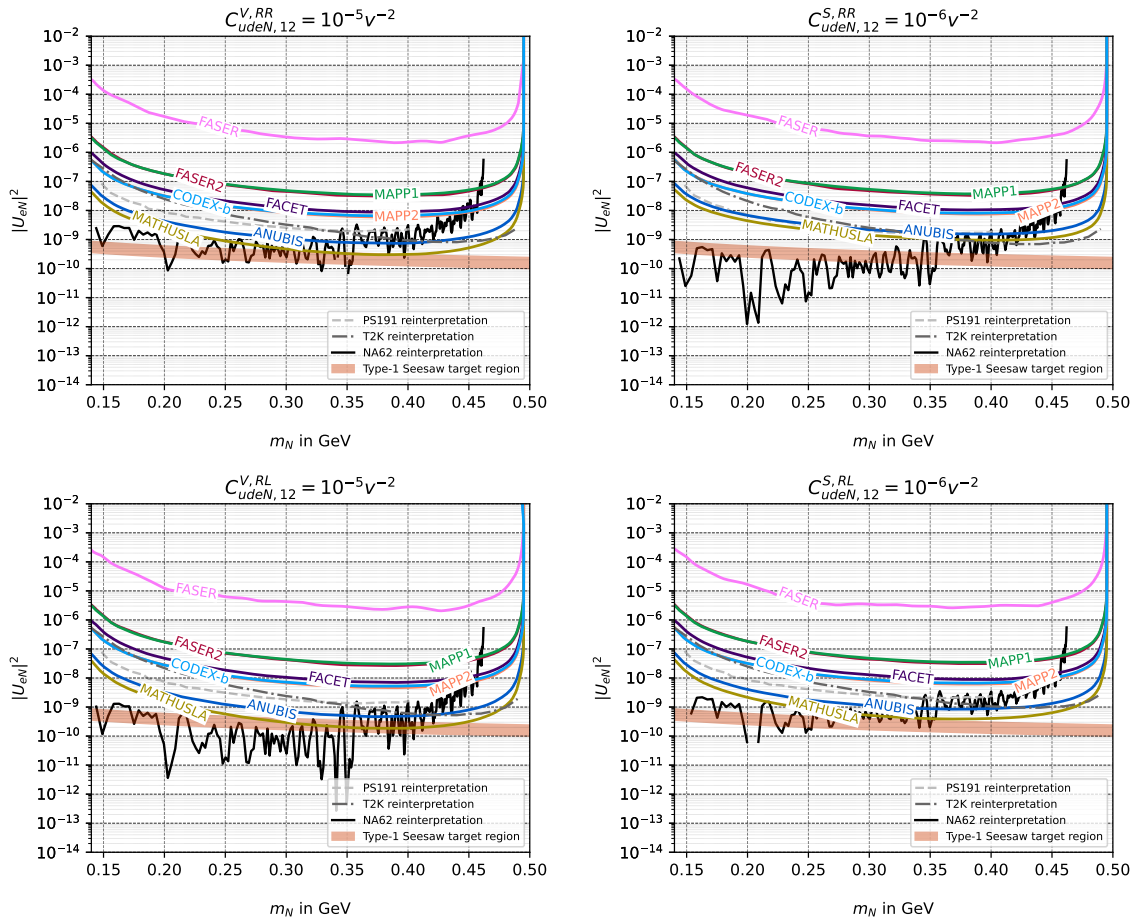


Figure 7. Projected exclusion limits in the plane $|U_{eN}|^2$ vs. m_N for single- N_R operator benchmarks B5 and B6 (top), and B7 and B8 (bottom). The absolute value of the corresponding WC has been fixed to $10^{-5}v^{-2}$ and $10^{-6}v^{-2}$ for vector and scalar operators, respectively. The recast bounds from NA62, T2K, and PS191 are also shown.

5 Summary

In this work, we have studied the potential of present and future far-detector experiments at the LHC for probing long-lived heavy neutral leptons (HNLs) of Majorana nature produced from rare kaon decays, in the theoretical framework of low-energy effective field theory extended with sterile neutrinos (N_R LEFT). We have focused on dimension-6 effective operators consisting of a pair of quarks together with a charged lepton and an HNL, or a pair of HNLs. Besides the effective operators, we also take into account the minimal mixing parameter between the HNLs and the standard-model active neutrinos. For simplicity, we assume in this work that there is only one kinematically relevant HNL, that the HNL mixes with the electron neutrino only, and that for the effective operators also only the first-generation leptons are considered.

There are both lepton-number-conserving and lepton-number-violating operators; we

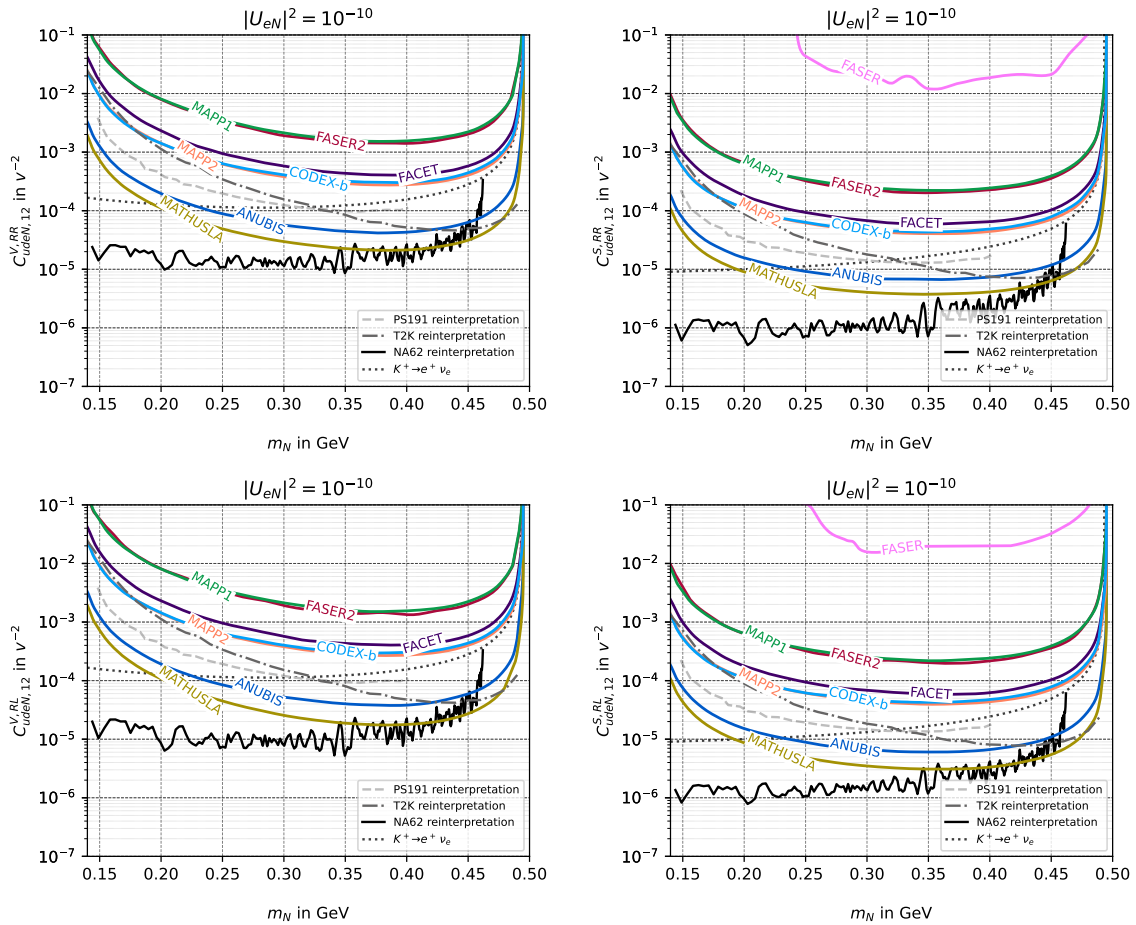


Figure 8. Exclusion limits in the plane WC vs. m_N for single- N_R operator benchmarks B5 and B6 (top), and B7 and B8 (bottom). The active-heavy neutrino mixing parameter has been fixed as $|U_{eN}|^2 = 10^{-10}$. The recast bounds from NA62, T2K, and PS191, as well as the constraint originating from the measured branching ratio of $K^+ \rightarrow e^+ \nu_e$, are also shown.

have investigated both of them and elaborated on their differences. We have computed the kaons' decay branching ratios into the HNLs with the considered effective operators, as a function of the HNL mass, the effective couplings, and the mixing parameter U_{eN} . In addition, the decay rates of the HNLs in the N_R LEFT are calculated with care, including the interference between the EFT operators and the minimal mixing contributions. We have further performed detailed Monte-Carlo simulations, in order to determine the acceptance of the far detectors for the long-lived HNLs. These experiments include ANUBIS, CODEX-b, FASER and FASER2, FACET, MATHUSLA, and MoEDAL-MAPP1 and MAPP2. In particular, because of the long-lifetime nature of the kaons (K^\pm , K_S , and K_L), we cannot assume they decay essentially at the interaction points; we have thus taken into account their decay positions in the simulation when we compute the decay probability of the HNLs in the detector fiducial volumes. Moreover, for the various experiments, we have properly placed a cut-off position beyond which the kaons are vetoed.

For a series of benchmark scenarios classified by the number of HNLs in the operators as well as the Lorentz structure of the operators, we have obtained numerical results. Besides the projection for the LHC far detectors, we have recast existing bounds on the HNLs in the minimal mixing scenario into those on the HNLs in the considered EFT benchmarks. We find that for the pair- N_R scenarios, the existing bounds from NA62 are already so strong that it has excluded all the parameter space that could be probed by future far-detector experiments. On the other hand, for the single- N_R benchmarks, the studied future experiments are sensitive to regions of parameter space currently unexcluded. Particularly, for benchmarks B3 and B4, the projected limits on the effective couplings can be orders of magnitude stronger than the existing bounds.

To summarize, our findings in this work show the potential of the proposed far detectors at the LHC for studying long-lived HNLs in the EFT framework, and highly motivate the construction and operation of the proposed far detectors at the LHC.

Acknowledgements

We thank Juan Carlos Helo and Felix Kling for useful discussions, and thank Giovanna Cottin for contributions in the early stage of the project. This work is supported by the Spanish grants PID2020-113775GB-I00 (AEI/10.13039/501100011033) and CIPROM/2021/054 (Generalitat Valenciana). R.B. acknowledges financial support from the Generalitat Valenciana (grant ACIF/2021/052).

A Kaon decays into HNLs

Throughout this work, we assume N to be a Majorana particle. We neglect $|\varepsilon| \ll 1$ responsible for indirect CP violation in the neutral kaon system, such that K_S and K_L coincide with K_1 and K_2 given by eq. (2.2). Since the latter are superpositions of flavor eigenstates and the effective operators we consider are written in the flavor basis, it proves convenient to define the following combinations of the Wilson coefficients:

$$a_{ij}^V \equiv c_{dN,ij}^{V,RR} - c_{dN,ij}^{V,LR} \quad \text{and} \quad a_{ij}^S \equiv c_{dN,ij}^{S,RR} - c_{dN,ij}^{S,LR}, \quad (\text{A.1})$$

$$b_{ij}^V \equiv c_{dN,ij}^{V,RR} + c_{dN,ij}^{V,LR} \quad \text{and} \quad b_{ij}^S \equiv c_{dN,ij}^{S,RR} + c_{dN,ij}^{S,LR}. \quad (\text{A.2})$$

In addition, for the single- N_R operators with a charged lepton, we define

$$c_{ij}^V \equiv c_{udeN,ij}^{V,RR} - c_{udeN,ij}^{V,LR} \quad \text{and} \quad c_{ij}^S \equiv c_{udeN,ij}^{S,RR} - c_{udeN,ij}^{S,LR}, \quad (\text{A.3})$$

$$d_{ij}^V \equiv c_{udeN,ij}^{V,RL} - c_{udeN,ij}^{V,LL} \quad \text{and} \quad d_{ij}^S \equiv c_{udeN,ij}^{S,RL} - c_{udeN,ij}^{S,LL}, \quad (\text{A.4})$$

$$g_{ij}^V \equiv c_{udeN,ij}^{V,RR} + c_{udeN,ij}^{V,LR} \quad \text{and} \quad g_{ij}^S \equiv c_{udeN,ij}^{S,RR} + c_{udeN,ij}^{S,LR}, \quad (\text{A.5})$$

$$h_{ij}^V \equiv c_{udeN,ij}^{V,RL} + c_{udeN,ij}^{V,LL} \quad \text{and} \quad h_{ij}^S \equiv c_{udeN,ij}^{S,RL} + c_{udeN,ij}^{S,LL}. \quad (\text{A.6})$$

Parameter	$f_+(0)$	Λ_+	$\log C$	$G(0)$	$B_T(0)/f_+(0)$	$s_T^{K\pi}$ [GeV ⁻²]
Central value	0.9706	0.02422	0.1198	0.0398	0.68	1.10

Table 5. Parameters entering the form factors f_+ , f_0 and B_T in eqs. (A.12)–(A.14).

A.1 Form factors

The non-zero hadronic matrix elements entering the computations of kaon decay amplitudes are given by

$$\langle 0 | \bar{s} \gamma^\mu \gamma_5 d | K^0 \rangle = i f_K p_K^\mu, \quad (\text{A.7})$$

$$\langle 0 | \bar{s} \gamma_5 d | K^0 \rangle = i \frac{m_K^2}{m_d + m_s} f_K \equiv i f_K^S, \quad (\text{A.8})$$

for leptonic kaon decays. Here $m_K = 493.6$ MeV is the neutral kaon mass, and $f_K = 155.7$ MeV [57], and f_K^S are the kaon decay constants. For $K^0 \rightarrow \pi^-$ transitions, the relevant matrix elements read

$$\langle \pi^- | \bar{s} \gamma^\mu u | K^0 \rangle = f_+(q^2) P^\mu + (f_0(q^2) - f_+(q^2)) \frac{m_K^2 - m_\pi^2}{q^2} q^\mu, \quad (\text{A.9})$$

$$\langle \pi^- | \bar{s} u | K^0 \rangle = \frac{m_K^2 - m_\pi^2}{m_u - m_s} f_0(q^2) \equiv f_S(q^2), \quad (\text{A.10})$$

$$\langle \pi^- | \bar{s} \sigma^{\mu\nu} u | K^0 \rangle = \frac{i}{m_K} (p_K^\mu p_\pi^\nu - p_K^\nu p_\pi^\mu) B_T(q^2), \quad (\text{A.11})$$

where $P = p_K + p_\pi$ is the sum of the kaon and pion 4-momenta, and $q = p_K - p_\pi$ is their difference. The three form factors (f_+ , f_0 , B_T) can be parameterized in terms of q^2 as follows (see Ref. [58] for more detail)

$$f_+(q^2) = f_+(0) + \Lambda_+ \frac{q^2}{m_\pi^2}, \quad (\text{A.12})$$

$$f_0(q^2) = f_+(0) + (\log C - G(0)) \frac{m_\pi^2}{m_K^2 - m_\pi^2} \frac{q^2}{m_\pi^2}, \quad (\text{A.13})$$

$$B_T(q^2) = B_T(0) (1 - s_T^{K\pi} q^2), \quad (\text{A.14})$$

and the numerical values of the parameters entering these expressions are reported in table 5.

A.2 Two-body decays

The partial decay widths of $K_{S/L} \rightarrow NN$ mediated by the pair- N_R operators \mathcal{O}_{dN} given in table 1 read:

$$\Gamma(K_S \rightarrow NN) = \frac{m_K}{32\pi} \sqrt{1 - \frac{4m_N^2}{m_K^2}} \left[4f_K^2 m_N^2 (\text{Im } a_{21}^V)^2 \right]$$

$$\begin{aligned}
& + (f_K^S)^2 \left\{ [\text{Im}(a_{21}^S - a_{12}^S)]^2 + [\text{Re}(a_{21}^S - a_{12}^S)]^2 \left(1 - \frac{4m_N^2}{m_K^2}\right) \right\} \\
& + 4f_K f_K^S m_N \text{Im} a_{21}^V \text{Im}(a_{21}^S - a_{12}^S) \Big], \tag{A.15}
\end{aligned}$$

$$\begin{aligned}
\Gamma(K_L \rightarrow NN) &= \frac{m_K}{32\pi} \sqrt{1 - \frac{4m_N^2}{m_K^2}} \left[4f_K^2 m_N^2 (\text{Re} a_{21}^V)^2 \right. \\
& + (f_K^S)^2 \left\{ [\text{Re}(a_{21}^S + a_{12}^S)]^2 + [\text{Im}(a_{21}^S + a_{12}^S)]^2 \left(1 - \frac{4m_N^2}{m_K^2}\right) \right\} \\
& \left. + 4f_K f_K^S m_N \text{Re} a_{21}^V \text{Re}(a_{21}^S + a_{12}^S) \right]. \tag{A.16}
\end{aligned}$$

In this computation, we have neglected the contribution from active-heavy mixing for two reasons: (i) the amplitude for $K_{S/L} \rightarrow NN$ is proportional to $U_{\ell N}^2$ and $|U_{\ell N}|^2 \ll 1$, and (ii) flavor-changing neutral currents are further suppressed, since in the SM they do not occur at tree level.

The single- N_R operators with a charged lepton summarized in table 2 as well as the standard active-heavy neutrino mixing trigger $K^- \rightarrow \ell^- N$. For the corresponding decay width, we find

$$\begin{aligned}
\Gamma(K^- \rightarrow \ell^- N) &= \frac{\lambda^{1/2}(m_K^2, m_\ell^2, m_N^2)}{64\pi m_K^3} \left\{ f_K^2 \left(|c_{12}^V|^2 + |d_{12}^V|^2 + |c_{\text{mix}}|^2 - 2 \text{Re}(d_{12}^V c_{\text{mix}}^*) \right) \right. \\
& \times \left[m_K^2 (m_\ell^2 + m_N^2) - (m_\ell^2 - m_N^2)^2 \right] \\
& + (f_K^S)^2 \left(|c_{12}^S|^2 + |d_{12}^S|^2 \right) [m_K^2 - m_\ell^2 - m_N^2] \\
& + 2f_K f_K^S \text{Re}(c_{12}^V c_{12}^{S*} + d_{12}^V d_{12}^{S*} - d_{12}^{S*} c_{\text{mix}}) m_\ell [m_K^2 - m_\ell^2 + m_N^2] \\
& - 4f_K^2 \text{Re}(c_{12}^V d_{12}^{V*} - c_{12}^V c_{\text{mix}}^*) m_K^2 m_\ell m_N - 4(f_K^S)^2 \text{Re}(c_{12}^S d_{12}^{S*}) m_\ell m_N \\
& \left. - 2f_K f_K^S \text{Re}(c_{12}^V d_{12}^{S*} + c_{12}^S d_{12}^{V*} - c_{12}^S c_{\text{mix}}^*) m_N [m_K^2 + m_\ell^2 - m_N^2] \right\}, \tag{A.17}
\end{aligned}$$

where $\lambda(x, y, z) = x^2 + y^2 + z^2 - 2xy - 2xz - 2yz$. This result complements eq. (52) of Ref. [23], where only one LNV operator ($C_{\text{VLL}}^{(6)}$ in their notation) arising from the N_R SMEFT at $d = 6$ has been included. In our notation, it means $d_{12}^V = -c_{udeN,12}^{V,LL}$ and $d_{12}^S = 0$. We find agreement with eq. (52) of Ref. [23] in this limit.

A.3 Three-body decays

We rely on the isospin symmetry and express the results in terms of the form factors f_+ , f_0 , f_S and B_T for $\langle \pi^- | \bar{s} \Gamma u | K^0 \rangle$ given in eqs. (A.12)–(A.14). By the isospin symmetry, we have

$$\langle \pi^0 | \bar{s} \Gamma d | K^0 \rangle = -\frac{1}{\sqrt{2}} \langle \pi^- | \bar{s} \Gamma u | K^0 \rangle, \tag{A.18}$$

$$\langle \pi^+ | \bar{s} \Gamma d | K^+ \rangle = \langle \pi^- | \bar{s} \Gamma u | K^0 \rangle. \tag{A.19}$$

The amplitude for $K_{S/L} \rightarrow \pi^0 NN$ is given by

$$\begin{aligned} \mathcal{M}(K_{S/L} \rightarrow \pi^0 NN) &= \frac{1}{4} (b_{21}^V \pm b_{21}^{V*}) \left[f_+ P_\mu + (f_0 - f_+) \frac{m_K^2 - m_\pi^2}{q^2} q_\mu \right] [\bar{u}_N \gamma^\mu \gamma_5 v_{N'}] \\ &+ \frac{f_S}{2} (b_{21}^S \mp b_{12}^S) [\bar{u}_N P_R v_{N'}] + \frac{f_S}{2} (b_{12}^S \mp b_{21}^S)^* [\bar{u}_N P_L v_{N'}] . \end{aligned} \quad (\text{A.20})$$

The squared amplitudes summed over spins then read:

$$\begin{aligned} \sum_{\text{spins}} |\mathcal{M}(K_S \rightarrow \pi^0 NN)|^2 &= 2 (\text{Re } b_{21}^V)^2 \left\{ -4f_+^2 (p \cdot p_N)^2 + 2f_+^2 (a + m_K^2 - m_\pi^2) (p \cdot p_N) \right. \\ &- f_+^2 [a(m_K^2 + m_N^2) - 2m_N^2(m_K^2 + m_\pi^2)] + \frac{(f_0^2 - f_+^2)}{a} m_N^2 (m_K^2 - m_\pi^2)^2 \left. \right\} \\ &+ \frac{f_S^2}{2} \left\{ [\text{Re}(b_{21}^S - b_{12}^S)]^2 a + [\text{Im}(b_{21}^S - b_{12}^S)]^2 (a - 4m_N^2) \right\} \\ &+ 2f_0 f_S m_N (m_K^2 - m_\pi^2) \text{Re } b_{21}^V \text{Re}(b_{21}^S - b_{12}^S) , \end{aligned} \quad (\text{A.21})$$

$$\begin{aligned} \sum_{\text{spins}} |\mathcal{M}(K_L \rightarrow \pi^0 NN)|^2 &= 2 (\text{Im } b_{21}^V)^2 \left\{ -4f_+^2 (p \cdot p_N)^2 + 2f_+^2 (a + m_K^2 - m_\pi^2) (p \cdot p_N) \right. \\ &- f_+^2 [a(m_K^2 + m_N^2) - 2m_N^2(m_K^2 + m_\pi^2)] + \frac{(f_0^2 - f_+^2)}{a} m_N^2 (m_K^2 - m_\pi^2)^2 \left. \right\} \\ &+ \frac{f_S^2}{2} \left\{ [\text{Im}(b_{21}^S + b_{12}^S)]^2 a + [\text{Re}(b_{21}^S + b_{12}^S)]^2 (a - 4m_N^2) \right\} \\ &+ 2f_0 f_S m_N (m_K^2 - m_\pi^2) \text{Im } b_{21}^V \text{Im}(b_{21}^S + b_{12}^S) . \end{aligned} \quad (\text{A.22})$$

For $K^+ \rightarrow \pi^+ NN$, we find:

$$\begin{aligned} \mathcal{M}(K^+ \rightarrow \pi^+ NN) &= \frac{b_{21}^V}{2} \left[f_+ P_\mu + (f_0 - f_+) \frac{M^2 - m^2}{q^2} q_\mu \right] [\bar{u}_N \gamma^\mu \gamma_5 v_{N'}] \\ &+ f_S b_{21}^S [\bar{u}_N P_R v_{N'}] + f_S b_{12}^{S*} [\bar{u}_N P_L v_{N'}] , \end{aligned} \quad (\text{A.23})$$

and

$$\begin{aligned} \sum_{\text{spins}} |\mathcal{M}(K^+ \rightarrow \pi^+ NN)|^2 &= 2 |b_{21}^V|^2 \left\{ -4f_+^2 (p \cdot p_N)^2 + 2f_+^2 (a + m_K^2 - m_\pi^2) (p \cdot p_N) \right. \\ &- f_+^2 [a(m_K^2 + m_N^2) - 2m_N^2(m_K^2 + m_\pi^2)] + \frac{(f_0^2 - f_+^2)}{a} m_N^2 (m_K^2 - m_\pi^2)^2 \left. \right\} \\ &+ f_S^2 \left\{ (|b_{21}^S|^2 + |b_{12}^S|^2) (a - 2m_N^2) - 4m_N^2 \text{Re}(b_{21}^S b_{12}^S) \right\} \\ &+ 2f_0 f_S m_N (m_K^2 - m_\pi^2) \text{Re} [b_{21}^V (b_{21}^{S*} - b_{12}^S)] . \end{aligned} \quad (\text{A.24})$$

Turning to the single- N_R operators with a charged lepton, we have

$$\mathcal{M}(K^- \rightarrow \pi^0 \ell^- N) = \frac{1}{2\sqrt{2}} \left\{ g_{12}^V [\bar{u}_\ell \gamma^\mu P_R v_N] + (h_{12}^V + c_{\text{mix}}) [\bar{u}_\ell \gamma^\mu P_L v_N] \right\}$$

$$\begin{aligned}
& \times \left[f_+ P_\mu + (f_0 - f_+) \frac{m_K^2 - m_\pi^2}{q^2} q_\mu \right] \\
& + \frac{f_S}{2\sqrt{2}} \left\{ g_{12}^S [\bar{u}_\ell P_R v_N] + h_{12}^S [\bar{u}_\ell P_L v_N] \right\} \\
& + \frac{i}{2\sqrt{2}} \frac{B_T}{m_K} \left\{ \left[p^\mu p^\nu - p^\nu p^\mu + i \epsilon_{\mu\nu\alpha\beta} p^\alpha p'^\beta \right] c_{udeN,12}^{T,RR} [\bar{u}_\ell \sigma^{\mu\nu} P_R v_N] \right. \\
& \left. + \left[p^\mu p^\nu - p^\nu p^\mu - i \epsilon_{\mu\nu\alpha\beta} p^\alpha p'^\beta \right] c_{udeN,12}^{T,LL} [\bar{u}_\ell \sigma^{\mu\nu} P_L v_N] \right\}. \quad (\text{A.25})
\end{aligned}$$

Finally, up to an unphysical sign,

$$\mathcal{M}(K_{S/L} \rightarrow \pi^+ \ell^- N) = \mathcal{M}(K^- \rightarrow \pi^0 \ell^- N). \quad (\text{A.26})$$

We do not provide the full expression for the modulus square of amplitude (A.25) summed over spins, since it is rather cumbersome. However, it is straightforward to obtain it, especially, assuming only one operator (either V, S, or T) at a time. In the limit of zero mixing ($c_{\text{mix}} = 0$), as in the case of two-body decay in eq. (A.17), the LNV single- N_R operators (switched on one at a time) lead to the same results as their LNC counterparts. Finally, the three-body decay widths are computed following the procedure explained in Refs. [23, 24].

B HNL decays

Effective operators in $N_R\text{LEFT}$ not only enhance the HNL production but also trigger their decay. Assuming only one generation of N_R , the pair- N_R operators in table 1 cannot make the HNL decay, whereas the single- N_R operators in table 2 do contribute to it. In this appendix we provide the partial decay width of $N \rightarrow \ell^- \pi^+$, which is the only kinematically allowed channel if HNLs are produced in kaon decays and if $m_N > m_\pi + m_\ell$. In the computation we take into account the contribution from (i) the \mathcal{O}_{udeN} operators in table 2, (ii) eq. (2.4), *i.e.* the standard mixing to active neutrinos, and (iii) the interference terms between (i) and (ii). The final expression reads

$$\begin{aligned}
\Gamma(N \rightarrow \ell^- \pi^+) &= \frac{\lambda^{1/2}(m_N^2, m_\ell^2, m_\pi^2)}{128\pi m_N^3} \left\{ f_\pi^2 \left(|c_{11}^V|^2 + |d_{11}^V|^2 + |c_{\text{mix}}|^2 - 2 \text{Re}(d_{11}^V c_{\text{mix}}^*) \right) \right. \\
& \times \left[(m_\ell^2 - m_N^2)^2 - m_\pi^2 (m_\ell^2 + m_N^2) \right] \\
& + (f_\pi^S)^2 \left(|c_{11}^S|^2 + |d_{11}^S|^2 \right) [m_\ell^2 + m_N^2 - m_\pi^2] \\
& - 2f_\pi f_\pi^S \text{Re}(c_{11}^V c_{11}^{S*} + d_{11}^V d_{11}^{S*} - c_{\text{mix}} d_{11}^{S*}) m_\ell [m_\ell^2 - m_N^2 - m_\pi^2] \\
& + 4f_\pi^2 \text{Re}(c_{11}^V d_{11}^{V*} - c_{11}^V c_{\text{mix}}^*) m_\pi^2 m_\ell m_N + 4(f_\pi^S)^2 \text{Re}(c_{11}^S d_{11}^{S*}) m_\ell m_N \\
& \left. - 2f_\pi f_\pi^S \text{Re}(c_{11}^V d_{11}^{S*} + c_{11}^S d_{11}^{V*} - c_{11}^S c_{\text{mix}}^*) m_N [m_\ell^2 - m_N^2 + m_\pi^2] \right\}. \quad (\text{B.1})
\end{aligned}$$

The previous result can be derived from the amplitude leading to eq. (A.17) by substituting K with π and performing the interchange $p_\pi \leftrightarrow p_N$ along the computation. The decay

constants are given by $f_\pi = 130.2 \text{ MeV}$ [57] and $f_\pi^S = \frac{m_\pi^2}{m_u + m_d} f_\pi$. We have also used the notation introduced in appendix A for the WC, and c_{mix} is the coefficient defined in eq. (2.5).

In the scenarios outlined in table 4, the decay of the HNL is governed by either the neutrino mixing parameter (scenarios B1–B2 and B5–B8) or one of the WC of the effective operators (scenarios B3 and B4). In cases where the former applies, eq. (B.1) reduces to the one in the minimal scenario [59]. Conversely, in the latter cases, eq. (B.1) can be simplified to

$$\begin{aligned} \Gamma(N \rightarrow \ell^- \pi^+) = & \frac{\lambda^{1/2} (m_N^2, m_\ell^2, m_\pi^2)}{128\pi m_N^3} \left\{ f_\pi^2 \left(|c_{11}^V|^2 + |d_{11}^V|^2 \right) \left[(m_\ell^2 - m_N^2)^2 - m_\pi^2 (m_\ell^2 + m_N^2) \right] \right. \\ & + (f_\pi^S)^2 \left(|c_{11}^S|^2 + |d_{11}^S|^2 \right) [m_\ell^2 + m_N^2 - m_\pi^2] \\ & + 4f_\pi^2 \text{Re} (c_{11}^V d_{11}^{V*}) m_\pi^2 m_\ell m_N + 4 (f_\pi^S)^2 \text{Re} (c_{11}^S d_{11}^{S*}) m_\ell m_N \\ & - 2f_\pi f_\pi^S \text{Re} (c_{11}^V c_{11}^{S*} + d_{11}^V d_{11}^{S*}) m_\ell [m_\ell^2 - m_N^2 - m_\pi^2] \\ & \left. - 2f_\pi f_\pi^S \text{Re} (c_{11}^V d_{11}^{S*} + c_{11}^S d_{11}^{V*}) m_N [m_\ell^2 - m_N^2 + m_\pi^2] \right\}. \end{aligned} \quad (\text{B.2})$$

It is worth mentioning that in scenarios B1–B2 and B5–B8, there are additional decay channels for N , such as the purely leptonic $\nu\nu\nu$ and $\nu\ell\ell$ channels, which enhance the HNL total decay width. The possible open channels depend on the HNL mass [59]. Meanwhile, in scenarios B3–B4, the total decay width becomes twice the result in eq. (B.2), since the charge conjugated channel is also open for Majorana N .

References

- [1] D. Curtin et al., *Long-Lived Particles at the Energy Frontier: The MATHUSLA Physics Case*, *Rept. Prog. Phys.* **82** (2019) 116201 [1806.07396].
- [2] J. Alimena et al., *Searching for long-lived particles beyond the Standard Model at the Large Hadron Collider*, *J. Phys. G* **47** (2020) 090501 [1903.04497].
- [3] J.L. Feng et al., *The Forward Physics Facility at the High-Luminosity LHC*, *J. Phys. G* **50** (2023) 030501 [2203.05090].
- [4] J.L. Feng, I. Galon, F. Kling and S. Trojanowski, *ForwArd Search ExpeRiment at the LHC*, *Phys. Rev. D* **97** (2018) 035001 [1708.09389].
- [5] FASER collaboration, *FASER’s physics reach for long-lived particles*, *Phys. Rev. D* **99** (2019) 095011 [1811.12522].
- [6] J.L. Pinfold, *The MoEDAL Experiment at the LHC—A Progress Report*, *Universe* **5** (2019) 47.
- [7] J.L. Pinfold, *The MoEDAL experiment: a new light on the high-energy frontier*, *Phil. Trans. Roy. Soc. Lond. A* **377** (2019) 20190382.
- [8] M. Bauer, O. Brandt, L. Lee and C. Ohm, *ANUBIS: Proposal to search for long-lived neutral particles in CERN service shafts*, 1909.13022.

- [9] V.V. Gligorov, S. Knapen, M. Papucci and D.J. Robinson, *Searching for Long-lived Particles: A Compact Detector for Exotics at LHCb*, *Phys. Rev. D* **97** (2018) 015023 [1708.09395].
- [10] S. Cerci et al., *FACET: A new long-lived particle detector in the very forward region of the CMS experiment*, *JHEP* **2022** (2022) 110 [2201.00019].
- [11] J.P. Chou, D. Curtin and H.J. Lubatti, *New Detectors to Explore the Lifetime Frontier*, *Phys. Lett. B* **767** (2017) 29 [1606.06298].
- [12] MATHUSLA collaboration, *An Update to the Letter of Intent for MATHUSLA: Search for Long-Lived Particles at the HL-LHC*, 2009.01693.
- [13] C. Antel et al., *Feebly Interacting Particles: FIPs 2022 workshop report*, in *Workshop on Feebly-Interacting Particles*, 5, 2023 [2305.01715].
- [14] F. del Aguila, S. Bar-Shalom, A. Soni and J. Wudka, *Heavy Majorana Neutrinos in the Effective Lagrangian Description: Application to Hadron Colliders*, *Phys. Lett. B* **670** (2009) 399 [0806.0876].
- [15] A. Aparici, K. Kim, A. Santamaria and J. Wudka, *Right-handed neutrino magnetic moments*, *Phys. Rev. D* **80** (2009) 013010 [0904.3244].
- [16] S. Bhattacharya and J. Wudka, *Dimension-seven operators in the standard model with right handed neutrinos*, *Phys. Rev. D* **94** (2016) 055022 [1505.05264].
- [17] Y. Liao and X.-D. Ma, *Operators up to Dimension Seven in Standard Model Effective Field Theory Extended with Sterile Neutrinos*, *Phys. Rev. D* **96** (2017) 015012 [1612.04527].
- [18] R. Beltrán, R. Cepedello and M. Hirsch, *Tree-level UV completions for N_R SMEFT $d = 6$ and $d = 7$ operators*, *JHEP* **08** (2023) 166 [2306.12578].
- [19] G. Cottin, J.C. Helo, M. Hirsch, A. Titov and Z.S. Wang, *Heavy neutral leptons in effective field theory and the high-luminosity LHC*, *JHEP* **09** (2021) 039 [2105.13851].
- [20] R. Beltrán, G. Cottin, J.C. Helo, M. Hirsch, A. Titov and Z.S. Wang, *Long-lived heavy neutral leptons at the LHC: four-fermion single- N_R operators*, *JHEP* **01** (2022) 044 [2110.15096].
- [21] W. Liu and Y. Zhang, *Testing neutrino dipole portal by long-lived particle detectors at the LHC*, *Eur. Phys. J. C* **83** (2023) 568 [2302.02081].
- [22] F. Delgado, L. Duarte, J. Jones-Perez, C. Manrique-Chavil and S. Peña, *Assessment of the dimension-5 seesaw portal and impact of exotic Higgs decays on non-pointing photon searches*, *JHEP* **09** (2022) 079 [2205.13550].
- [23] J. De Vries, H.K. Dreiner, J.Y. Günther, Z.S. Wang and G. Zhou, *Long-lived Sterile Neutrinos at the LHC in Effective Field Theory*, *JHEP* **03** (2021) 148 [2010.07305].
- [24] R. Beltrán, G. Cottin, J.C. Helo, M. Hirsch, A. Titov and Z.S. Wang, *Long-lived heavy neutral leptons from mesons in effective field theory*, *JHEP* **01** (2023) 015 [2210.02461].
- [25] D. Barducci, E. Bertuzzo, M. Taoso and C. Toni, *Probing right-handed neutrinos dipole operators*, *JHEP* **03** (2023) 239 [2209.13469].
- [26] D. Barducci, W. Liu, A. Titov, Z.S. Wang and Y. Zhang, *Probing the dipole portal to heavy neutral leptons via meson decays at the high-luminosity LHC*, 2308.16608.

- [27] I. Bischer and W. Rodejohann, *General neutrino interactions from an effective field theory perspective*, *Nucl. Phys. B* **947** (2019) 114746 [1905.08699].
- [28] M. Chala and A. Titov, *One-loop matching in the SMEFT extended with a sterile neutrino*, *JHEP* **05** (2020) 139 [2001.07732].
- [29] T. Li, X.-D. Ma and M.A. Schmidt, *General neutrino interactions with sterile neutrinos in light of coherent neutrino-nucleus scattering and meson invisible decays*, *JHEP* **07** (2020) 152 [2005.01543].
- [30] T. Li, X.-D. Ma and M.A. Schmidt, *Constraints on the charged currents in general neutrino interactions with sterile neutrinos*, *JHEP* **10** (2020) 115 [2007.15408].
- [31] G. Zhou, J.Y. Günther, Z.S. Wang, J. de Vries and H.K. Dreiner, *Long-lived sterile neutrinos at Belle II in effective field theory*, *JHEP* **04** (2022) 057 [2111.04403].
- [32] T. Han, J. Liao, H. Liu and D. Marfatia, *Right-handed Dirac and Majorana neutrinos at Belle II*, *JHEP* **04** (2023) 013 [2207.07029].
- [33] A. Abada, D. Bečirević, O. Sumensari, C. Weiland and R. Zukanovich Funchal, *Sterile neutrinos facing kaon physics experiments*, *Phys. Rev. D* **95** (2017) 075023 [1612.04737].
- [34] T. Li, X.-D. Ma and M.A. Schmidt, *Implication of $K \rightarrow \pi\nu\bar{\nu}$ for generic neutrino interactions in effective field theories*, *Phys. Rev. D* **101** (2020) 055019 [1912.10433].
- [35] G. Zhou, *Light sterile neutrinos and lepton-number-violating kaon decays in effective field theory*, *JHEP* **06** (2022) 127 [2112.00767].
- [36] E. Fernández-Martínez, M. González-López, J. Hernández-García, M. Hostert and J. López-Pavón, *Effective portals to heavy neutral leptons*, *JHEP* **09** (2023) 001 [2304.06772].
- [37] A.J. Buras, *Weak Hamiltonian, CP violation and rare decays*, in *Les Houches Summer School in Theoretical Physics, Session 68: Probing the Standard Model of Particle Interactions*, pp. 281–539, 6, 1998 [hep-ph/9806471].
- [38] PARTICLE DATA GROUP collaboration, *Review of Particle Physics*, *PTEP* **2022** (2022) 083C01.
- [39] NA62 collaboration, *Search for heavy neutral lepton production in K^+ decays to positrons*, *Phys. Lett. B* **807** (2020) 135599 [2005.09575].
- [40] G. Bernardi et al., *Further limits on heavy neutrino couplings*, *Phys. Lett. B* **203** (1988) 332.
- [41] T2K collaboration, *Search for heavy neutrinos with the T2K near detector ND280*, *Phys. Rev. D* **100** (2019) 052006 [1902.07598].
- [42] PIENU collaboration, *Improved search for heavy neutrinos in the decay $\pi \rightarrow e\nu$* , *Phys. Rev. D* **97** (2018) 072012 [1712.03275].
- [43] L.D. Corpe, “Update on (pro)ANUBIS detector proposal: https://indico.cern.ch/event/1216822/contributions/5449255/attachments/2671754/4631593/LCORPE_LLWorkshop2023_ANUBIS_June2023.pdf.”, June, 2023.
- [44] T.P. Satterthwaite, *Sensitivity of the ANUBIS and ATLAS Detectors to Neutral Long-Lived Particles Produced in pp Collisions at the Large Hadron Collider*, Master’s thesis, 2022.

- [45] FASER collaboration, *First Direct Observation of Collider Neutrinos with FASER at the LHC*, [2303.14185](#).
- [46] FASER collaboration, *First Physics Results from the FASER Experiment*, in *57th Rencontres de Moriond on Electroweak Interactions and Unified Theories*, 5, 2023 [[2305.08665](#)].
- [47] L. Lee, C. Ohm, A. Soffer and T.-T. Yu, *Collider Searches for Long-Lived Particles Beyond the Standard Model*, *Prog. Part. Nucl. Phys.* **106** (2019) 210 [[1810.12602](#)].
- [48] T. Pierog, I. Karpenko, J.M. Katzy, E. Yatsenko and K. Werner, *EPOS LHC: Test of collective hadronization with data measured at the CERN Large Hadron Collider*, *Phys. Rev. C* **92** (2015) 034906 [[1306.0121](#)].
- [49] C. Baus, T. Pierog and R. Ulrich, “Cosmic Ray Monte Carlo (CRMC): <https://web.ikp.kit.edu/rulrich/crmc.html>.”, June, 2023.
- [50] D. Dercks, J. De Vries, H.K. Dreiner and Z.S. Wang, *R-parity Violation and Light Neutralinos at CODEX-b, FASER, and MATHUSLA*, *Phys. Rev. D* **99** (2019) 055039 [[1810.03617](#)].
- [51] D. Dercks, H.K. Dreiner, M. Hirsch and Z.S. Wang, *Long-Lived Fermions at AL3X*, *Phys. Rev. D* **99** (2019) 055020 [[1811.01995](#)].
- [52] M. Hirsch and Z.S. Wang, *Heavy neutral leptons at ANUBIS*, *Phys. Rev. D* **101** (2020) 055034 [[2001.04750](#)].
- [53] J.Y. Günther, J. de Vries, H.K. Dreiner, Z.S. Wang and G. Zhou, *Long-lived neutral fermions at the DUNE near detector*, [2310.12392](#).
- [54] R. Beltrán, G. Cottin, M. Hirsch, A. Titov and Z.S. Wang, *Reinterpretation of searches for long-lived particles from meson decays*, *JHEP* **05** (2023) 031 [[2302.03216](#)].
- [55] H.K. Dreiner, D. Köhler, S. Nangia, M. Schürmann and Z.S. Wang, *Recasting bounds on long-lived heavy neutral leptons in terms of a light supersymmetric R-parity violating neutralino*, *JHEP* **08** (2023) 058 [[2306.14700](#)].
- [56] R. Barouki, G. Marocco and S. Sarkar, *Blast from the past II: Constraints on heavy neutral leptons from the BEBC WA66 beam dump experiment*, *SciPost Phys.* **13** (2022) 118 [[2208.00416](#)].
- [57] FLAVOUR LATTICE AVERAGING GROUP (FLAG) collaboration, *FLAG Review 2021*, *Eur. Phys. J. C* **82** (2022) 869 [[2111.09849](#)].
- [58] A. Falkowski, M. González-Alonso, J. Kopp, Y. Soreq and Z. Tabrizi, *EFT at FASER ν* , *JHEP* **10** (2021) 086 [[2105.12136](#)].
- [59] K. Bondarenko, A. Boyarsky, D. Gorbunov and O. Ruchayskiy, *Phenomenology of GeV-scale Heavy Neutral Leptons*, *JHEP* **11** (2018) 032 [[1805.08567](#)].